https://doi.org/10.5194/wes-2025-100
Preprint. Discussion started: 30 June 2025

eawe european academy of wind energy
Open Access WIND ENERGY SCIENCE DISCUSSIONS

On the development of a hardware-in-the-loop wind tunnel setup to study the aerodynamic response of floating offshore wind turbines

Federico Taruffi[1], Shakthi Thinakaran[1], and Axelle Viré[1]
[1]Faculty of Aerospace Engineering, Delft University of Technology, Kluyverweg 1, 2629 HS Delft, the Netherlands
Correspondence: Federico Taruffi (F.Taruffi@tudelft.nl)

Abstract.
In floating wind turbines, the met-ocean conditions lead to motions of the floater affecting the rotor aerodynamic loads, which in return influence the motion of the floater, in a highly coupled way. Numerical design tools have proven to fail to predict some aerodynamic phenomena, such as the increase in thrust variation caused by unsteady effects. Thus, experimental testing is essential for tuning and validating these codes. Hybrid testing in wind tunnels, by reproducing numerically and actuating the floater motions while measuring aerodynamic loads on a physical scale turbine model, overcomes the scaling issues of traditional wave basin tests allowing a higher fidelity in the reproduction of the aerodynamics. This work presents the development of a hybrid hardware-in-the-loop setup designed to study the aerodynamic response of floating wind turbines in wind tunnels. A scale model of a multi-megawatt floating wind turbine is mounted on top of a six degrees-of-freedom hexapod robot. The full coupling of aerodynamic and floater dynamics is obtained with a hardware-in-the-loop approach with force-feedback-motion-actuation architecture. The rotor loads measured on the physical rotor are fed into a floater dynamic numerical simulator which calculates the motion in real-time and actuates it through a moving platform called hexapod. Key outcomes include the development of a hardware-in-the-loop numerical model with a force correction method to cope with scaling effects and an assessment procedure to verify the simulator, correction model, and measurement-actuation chain. The aerodynamic effects on the motion response are preliminarily investigated on a 10MW floating concept, with direct estimation of the rotor aerodynamic damping showing a 210% increase of damping in pitch with the turbine in operation. The capability of testing combined wind and wave cases is also demonstrated, setting the framework for future studies.

1 Introduction

Offshore wind turbines are mostly installed as bottom-fixed structures rigidly mounted on the seabed or are moored to the seabed using floating support structures. In deeper waters exceeding 60 meters in depth, floating turbines anchored on the seabed are more economical (van Kuik et al., 2016). As suitable shallow-water sites become increasingly scarce, floating offshore wind turbines (FOWTs) offer a promising alternative, unlocking the potential to harness vast wind resources in deeper seas and opening new opportunities in countries without shallow seas.

FOWTs experience motions in six degrees-of-freedom (DOFs). The floating nature of the wind turbine makes it susceptible to various excitations, including changes in the met-ocean conditions, interactions between the wakes and the turbine, and the operation of the turbine itself. The aerodynamic performance of FOWTs is affected by these motions, with the aerodynamic loads acting on the rotor being highly coupled with the floater dynamics. In some cases, unsteady aerodynamic effects are observed due to the interaction of the wind turbine blades with their own wake. These complex interactions are often not yet fully understood.

It is currently challenging to numerically predict the unsteady aerodynamic loads under certain conditions. In previous studies (Taruffi et al., 2024b) the results from an experimental test were compared with the quasi-static theory which failed to predict the unsteady aerodynamic loading at high frequency. Discrepancies in predicting these unsteady loads were also found with high-fidelity numerical models, such as large-eddy simulations with an actuator line model (Taruffi et al., 2024a). In the field, some recently-deployed FOWTs also needed premature maintenance on their rotors. This shows the need to better understand the unsteady phenomena and derive more accurate numerical tools for the design of FOWTs.

Experimental testing provides an effective way to investigate these complex phenomena and tune the numerical models. Full-scale testing or large-scale model testing can be done at sea. This was done by Viselli et al. (2015) with a 1:8 FOWT in the Gulf of Maine and by Ruzzo et al. (2021) with a 1:15 floating multi-purpose-platform including a wind turbine. However, this is expensive and the real offshore conditions are difficult to reproduce numerically. Hence laboratory tests with scaled models are often preferred.

Testing FOWTs is traditionally done in a wave basin with Froude scaling. This allows for accurate hydrodynamic load reproduction, enabling the understanding of the floater hydrodynamics. For example, Cermelli and Aubault (2010) studied the hydrodynamics of a 1:67 scaled FOWT in a wave basin with Froude scaling to validate a numerical model. In order to include aerodynamic loading, wind generators with thrust disks or geometrically scaled blades were used to emulate the aerodynamic thrust force on the rotor. These methods successfully generated an aerodynamic thrust force but did not match the values of the full-scale model. The study by Goupee et al. (2014b) that involved testing a 5 MW wind turbine with different floaters in a wave basin with geometrically scaled blades revealed their drawbacks . This is due to the use of the Froude scaling law that does not allow for reproducing the aerodynamic forces correctly (Robertson et al., 2013). A Reynolds' similarity law does allow for accurate representation of the aerodynamics but it compromises the hydrodynamics and gravity related loads and also leads to impossibly high wind speeds. This scaling law conflict is unavoidable in fully-physical wave basin scale tests. To alleviate it, later studies followed a performance-based scaling methodology for the rotor by choosing an arbitrary velocity scaling factor for reproducing aerodynamic thrust more accurately while keeping the Froude scaling for the structure (Goupee et al., 2014a; Zhao et al., 2018; Doisenbant et al., 2018). However, this approach still has limitations. The wind generators only produce low-quality wind flows, and the correct mass scaling is not achievable in the turbine leading to an inaccurate centre of gravity.

Hybrid testing overcomes these challenges. Instead of physically applying both the aerodynamic and hydrodynamic loading, one part is physically tested while the other is numerically simulated, effectively eliminating the scaling conflict. This can be done in wave basins where aerodynamic thrust is simulated with the help of winches or thrusters, or in a wind tunnel where an actuated platform is used to behave as the floater. The choice depends on the scope of the study, with the wave basin and wind tunnel setups meant to perform studies on hydrodynamics and aerodynamics respectively. Due to the high level of coupling between the aerodynamic loads acting on the rotor, and the motion response of the floating system, hybrid tests where the numerical part contribution is pre-calculated may be suitable for specific studies but are not suitable to truly reproduce realistic conditions that are necessary to investigate the aerodynamic response and the stability of a design solution. To allow this, hardware-in-the-loop (HIL) technology is used, where the numerical part is simulated in real-time and accounts for the real-time measurements from the physical model to emulate the missing physics.

The first approach for real-time hybrid experimental testing in wave basins was developed with a ducted fan actuator by Azcona et al. (2014). The speed of the fan was adjusted to emulate different aerodynamic thrust forces. This methodology was later used to study the non-linear hydrodynamic effects of a FOWT as described in Azcona et al. (2019) and it overtook the traditional non-hybrid testing methods as it was confirmed to have better accuracy. Other researchers such as Oguz et al. (2018), Armesto et al. (2018) and Thys et al. (2018); Bachynski et al. (2016) developed it further to include multiple fans or winch cables in order to better emulate aerodynamic forces. These testing methods were used to verify and/or compare FOWT designs, observe complex interactions, or tune numerical codes.

The HIL setup in wave basins allowed for validating floater designs and studying the complex dynamics. However, to analyse aerodynamic effects such as unsteady aerodynamics and wake interactions, testing in a wind tunnel is required. Hybrid experimental testing in wind tunnels was pioneered by Belloli et al. (2020) who developed a HIL setup with a 10 MW thrust-scaled wind turbine model mounted on a two DOFs slide first (Bayati et al., 2017) and a six DOFs hexapod later (Bayati et al., 2018b). A numerical model was developed to solve the floater dynamics, but still with limited force feedback (Bayati et al., 2018a). Recently, a 15 MW FOWT was tested with a 1:100 length scale with the same setup (Fontanella et al., 2023b). Hybrid wind tunnel testing was also conducted by researchers such as Rockel et al. (2014) and Schliffke et al. (2020) to study the wake characteristics of FOWTs, however without hardware-in-loop coupling. They experimented with highly scaled models under prescribed motions in a boundary layer wind tunnel. Overall, research that used hybrid testing in wind tunnels to study FOWT dynamics is scarce.

In a previous work by Taruffi et al. (2024b), a setup was developed at Delft University of Technology for hybrid testing of FOWT in wind tunnel using a 6 DOFs hexapod robot. While that study used imposed motions, in this work the setup is further developed to investigate the aerodynamic response of FOWTs using HIL technology. The setup comprises physical aerodynamic loads that are fully coupled with numerically simulated floater dynamics. A numerical model is developed that solves the dynamics of the floater in 6 DOFs which includes correcting the measured force due to non-Froude scaling and simulating the waves. Due to the scaling mismatch, the reliability of the force correction plays an important role in the accuracy of the setup for simulating real-world dynamics. This work primarily focuses on the verification and validation of the setup, especially the force correction methodology, to ensure its accuracy to be utilised in future studies. An objective is to make the setup versatile enough to accommodate various FOWT designs, enabling the testing of larger turbines and different floater configurations with ease. Preliminary free decay and combined wind and wave tests are performed on a 10MW FOWT concept, investigating the aerodynamic damping effect on the motion response and assessing the capability of the setup to reproduce realistic wind and wave conditions.

https://doi.org/10.5194/wes-2025-100
Preprint. Discussion started: 30 June 2025

eawe european academy of wind energy
Open Access WIND ENERGY SCIENCE DISCUSSIONS

2 The hybrid setup

The hybrid setup comprises a wind turbine scale model - the physical subsystem - and a six degrees-of-freedom hexapod robot - the numerical subsystem. The skeleton of the setup is the same as the previous work (Taruffi et al., 2024b) which focused on the study of rotor unsteady aerodynamics. In addition to the previous setup, a real-time controller bridges the two subsystems to implement the hardware-in-the-loop functionality. This setup is for use in wind tunnels. For this work, it was tested in the Open Jet Facility (OJF) at the Delft University of Technology, a closed-loop open jet test section facility with a $2.85\mathrm{m} \times 2.85\mathrm{m}$ nozzle opening into a 13m long, 8m high open test section. At $1\mathrm{m}$ downstream the nozzle, where the rotor is placed, the flow is uniform with a turbulence intensity of 0.5%. A view of the hybrid setup in OJF, with its components highlighted, is shown in Fig. 1.

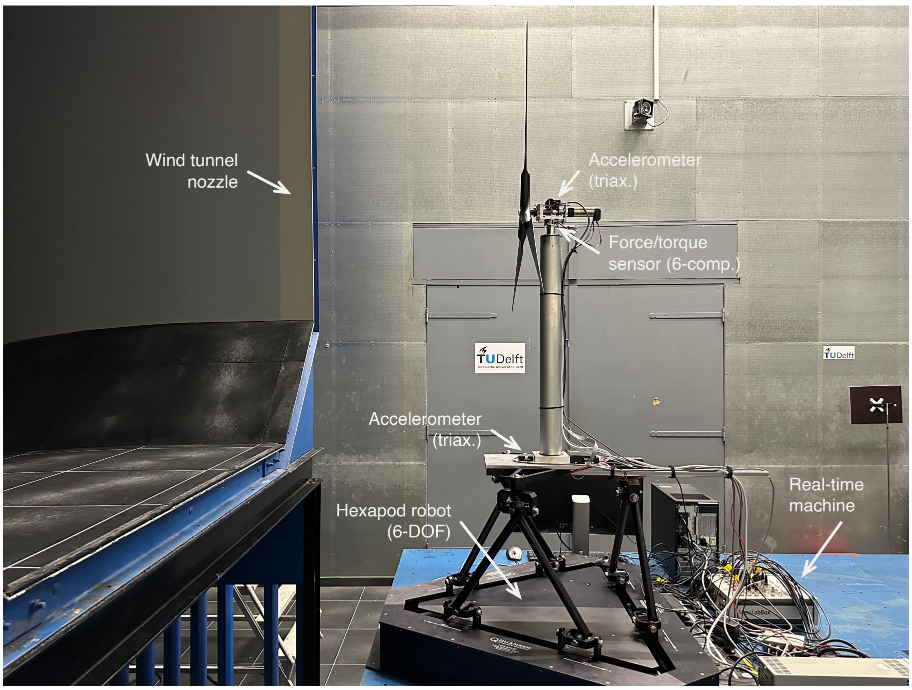

Figure 1. Picture of the setup and its components.

2.1 Wind turbine model

The scale wind turbine is a 3-bladed, fixed-pitch 1:148 model of the DTU 10 MW reference concept (Bak et al., 2013) operating with a velocity scale of 3. The rotor is scaled by Fontanella et al. (2023a) with a performance-scaling approach aimed at correctly reproducing the thrust force, which is a common scaling objective for floating-related test models due to the predominant role of thrust in FOWTs motion. A complete experimental aerodynamic assessment, including both static and dynamic conditions, was performed in the previous study (Taruffi et al., 2024b). The relevant properties are reported in Table 1. The ex-

https://doi.org/10.5194/wes-2025-100
Preprint. Discussion started: 30 June 2025

eawe european academy of wind energy
Open Access WIND ENERGY SCIENCE DISCUSSIONS

110 perimental thrust curve is shown in Fig. 2 and assesses the aerodynamic design of the rotor, proving its suitability to reproduce the full-scale rotor.

Table 1. Main wind turbine model specifications.

Parameter	Value	Unit
Length scale	148	-
Velocity scale	3	-
Rotor diameter	1.2	m
Hub height	0.8	m
Tilt angle	0	deg
Nacelle mass	1.03	kg
Rotor mass	0.58	kg
Rated wind speed	4	m/s
Rated rotor speed	480	rpm

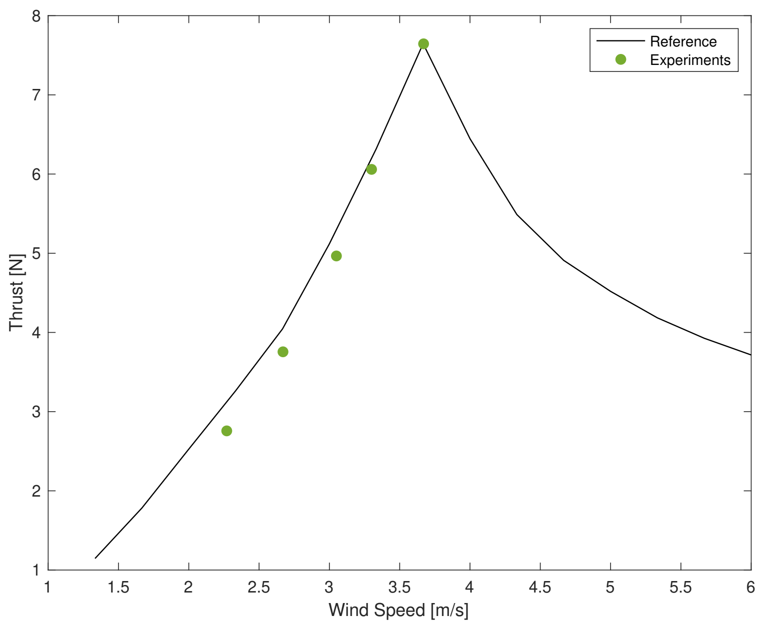

Figure 2. Rotor thrust from experiments (Taruffi et al., 2024b) compared with the nominal thrust curve of the full-scale turbine (reported at model-scale). The experimental points are averaged over two sets.

https://doi.org/10.5194/wes-2025-100
Preprint. Discussion started: 30 June 2025

2.2 Hexapod

The motion system is the commercially available parallel kinematics robot Quanser Hexapod. The maximum velocity and acceleration are $0.67\mathrm{m/s}$ and $9\mathrm{m/s^2}$ for translations and $80\mathrm{deg/s}$ and $800\mathrm{deg/s^2}$ for rotations. The capabilities and limitations of the hexapod were evaluated with tests in the previous study (Taruffi et al., 2024b). A key outcome for this application is that the hexapod can move the wind turbine at frequencies up to $5\mathrm{Hz}$ ($0.1\mathrm{Hz}$ at full-scale or 1.5 in terms of reduced frequency) without tracking errors. The frequency range and acceleration limits are within the scaled motion range of 10MW FOWTs for most load conditions.

2.3 Instrumentation

The instrumentation system consists of several sensors and a real-time controller. A six-component load cell (model ATI mini45 SI-290-10) installed between the tower top and the nacelle is used to measure the rotor integral loads and obtain the aerodynamic forces. Two MEMS triaxial low-frequency accelerometers (model TE Connectivity 4030-002-120), one placed at the hexapod-tower connection and the other one positioned on top of the nacelle, measure the translational accelerations. Both are used to verify motion tracking, and the one on the nacelle is also used, together with the load cell, for the rotor force correction process, as explained in Section 3.1.

The rotor is driven by a motor (model Maxon EC-4pole 30 200W) featuring a gearbox (model Maxon GP 32 C 5.8:1) and connected to the rotor shaft with an Oldham coupling. The motor is controlled at constant speed by a servo drive (model Maxon Escon 70/10) and equipped with a braking resistor (model Maxon DSR 70/30) to dissipate the power generated. The servo drive provides the wind turbine operating data of rotational speed, measured by an encoder (model HEDL 5540) at the motor, and torque, calculated from the motor current.

A real-time controller (model dSPACE 1302) is used to perform the hardware-in-the-loop, chaining measurements and actuation by simulating, in real-time, the floater dynamics (see Section 3). The unit is also used for data acquisition (DAQ) of all the sensor signals and as human-machine interface (HMI) to set test cases, command the operation of the turbine model and monitor the signals. The machine operates at $1\mathrm{kHz}$.

The wind speed is measured using a pitot tube installed in the tunnel nozzle. The speed at the testing location is also verified with a portable fan-type anemometer.

2.4 Scaling of FOWT concept

This hybrid setup is designed to be scalable and represent different FOWT systems in the size range of $10\mathrm{MW}$ with a scale around 1:150. The rotor is a scale model designed for the DTU 10 MW reference wind turbine, but it can represent other concepts like the NREL 5 MW or the IEA 15 MW by adjusting the operating parameters according to the scale, as their design is closely related. Since the floater is represented by a numerical model, it is virtually possible to use any platform and mooring design.

https://doi.org/10.5194/wes-2025-100
Preprint. Discussion started: 30 June 2025

As introduced in Section 1, one of the key drivers of hybrid testing is to be able to overcome the Froude-Reynolds scale conflict. For hybrid testing in wind tunnels, this translates into a custom scaling law (in Table 3) that comes as close as feasible to the Reynolds scale bearing limitations given by the facility and the model manufacturing.

A non-Froude scaling introduces an acceleration mismatch which results in an incorrect reproduction of inertial and gravitational phenomena acting on the wind turbine, while those acting on the floater are not affected as they are numerically reproduced. Moreover, a mass mismatch is hardly avoidable at these scales due to production constraints resulting in a manufacturable rotor-nacelle assembly mass around 10 times the scaled value. The combination of these scaling issues leads to large errors and has to be numerically compensated by the hardware-in-the-loop setup for a correct reproduction of the full-scale dynamics, as explained in Section 3.1.

A limitation on the size of the FOWT reproducible is given by the scaling. Representing bigger concepts with the same setup, as a 15 MW FOWT or more, increases the scaling effects. On the aerodynamic side, an increase in the Reynolds number mismatch with the scale worsens the performance of the rotor. On the actuation side, the motion needs to be quicker, approaching the limits of the hexapod in terms of motion frequency ($\lambda_f = \lambda_v \lambda_l^{-1}$) and also challenging the hardware-in-the-loop chain latency.

Ultimately, an openly available 10 MW FOWT concept is chosen in this work with the scope of verification of the setup itself. This is the DTU 10 MW with the SWE TripleSpar floater (Lemmer et al., 2016), whose design was validated in Bredmose et al. (2017). The relevant properties of the concept are in Table 2 and the resulting scale factors are in Table 3. The load cases used as reference for the wave tests were extracted from (Ramachandran et al., 2017) and refer to a site located in the Gulf of Maine.

https://doi.org/10.5194/wes-2025-100
Preprint. Discussion started: 30 June 2025

Table 2. Properties of the FOWT concept from Bak et al. (2013); Lemmer et al. (2016)

Parameter	Value	Unit
Rotor diameter	178.3	m
Hub height	94	m
Rated wind speed	11.4	m/s
Rated rotor speed	9.6	rpm
Rotor-nacelle-assembly mass	612350	kg
Rated thrust	1619	kN
Rated power	10	MW
Floater mass	28828000	kg
Floater inertia, x	1.8674×10^{10}	kgm^2
Floater inertia, y	1.8674×10^{10}	kgm^2
Floater inertia, z	2.0235×10^{10}	kgm^2
Platform surge natural frequency	0.005	Hz
Platform heave natural frequency	0.06	Hz
Platform pitch natural frequency	0.04	Hz

Table 3. Non-Froude custom scale factors calculation and values.

Factor	Symbol	Formula	Value (fs/ms)
Length	λ_l		148
Velocity	λ_v		3
Frequency	λ_f	$\lambda_l^{-1}\lambda_v$	0.02
Acceleration	λ_a	$\lambda_l\lambda_v^2$	0.06
Mass	λ_m	λ_l^3	3241792
Reynolds mismatch	λ_{Re}	$\lambda_l\lambda_v$	444

3 Hardware-in-the-loop

This setup's HIL architecture is of the type force-feedback-motion-actuation. The aerodynamic loads are measured on the physical model and are fed into the floater simulator, which calculates the next state of the system and actuates the hexapod, which moves accordingly. The floater simulator is a HIL numerical model developed in Matlab/Simulink environment to run in the real-time machine and it solves the dynamics of the floater in real-time by integrating the equation of motion at each time step, accounting for the measured aerodynamic loads, the numerically generated sea state and the hydrostatics, hydrodynamics and mooring system of the floater (see Section 3.2). The motions affect the measured aerodynamic loads, which in return affect

https://doi.org/10.5194/wes-2025-100
Preprint. Discussion started: 30 June 2025

the calculated motions at the next time step. This creates a loop and allows the two-way coupling of the rotor aerodynamics with the floater dynamic motions. A scheme of the HIL architecture is shown in Fig. 3.

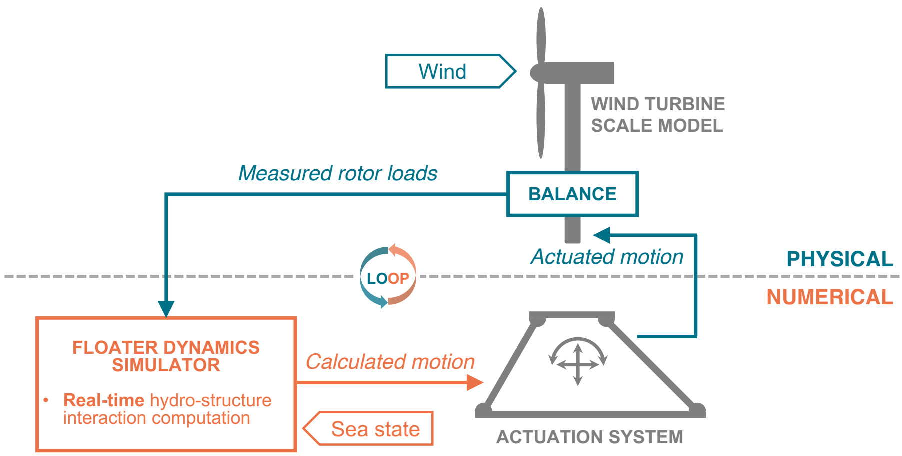

Figure 3. Scheme of the HIL architecture showing the force-feedback and motion-actuation chain.

3.1 Force correction

Measuring pure aerodynamic loads with a load cell is not feasible for dynamic applications such as the one of interest here. The load cell measures at least the entire rotor load and, depending on where it is positioned, also the nacelle and tower loads. This includes aerodynamic, inertial and gravitational contributions. Differently from Belloli et al. (2020), here the load cell used for the force-feedback is positioned between the tower top and the nacelle, instead of under the tower, and thus measures the loads acting on the rotor-nacelle assembly only. The advantage of measuring at the top of the tower is that the fraction of aerodynamic forces over measured forces is greater as the tower's inertial contributions, which are large given its non-scaled mass - the tower is designed as rigid - are not measured.

However, the measured rotor-nacelle forces cannot be directly used in the floater simulation and a correction procedure is necessary for two reasons. Firstly, the non-Froude scaling chosen for the setup (see Section 2.4) implies that the acceleration factor is not 1, thus the accelerations must be scaled. This applies also to the gravitational acceleration, which is not feasible to scale in experiments, leading to a gravitational acceleration mismatch. Secondly, the mass of the rotor and nacelle cannot be scaled correctly due to manufacturing constraints that make it unfeasible to manufacture respecting the mass scale for models in this scale range (1:100 - 1:200). This is due to the necessary utilization of commercial components - like actuators, sensors and mechanical components - and the need of preserving the structural functionality of the scaled model. These acceleration and mass mismatches result in the misrepresentation of gravitational and inertial forces in the experiments. Since these forces are read by the load cell together with the aerodynamic forces, which are not affected by misscaling, the measurements are heavily compromised. To give an order of magnitude of the impairment, the acceleration mismatch of 15 and the mass mismatch of 10

https://doi.org/10.5194/wes-2025-100
Preprint. Discussion started: 30 June 2025

lead to a mismatch in the ratio between the aerodynamic forces and the inertial and gravitational forces of 150. Aerodynamic forces and their effects being the focus of study in this setup, it is clear how this significant error would impair the experiments.

For this reason, a correction procedure is needed in real-time during the experiments. It was developed in this work, as described hereafter, and is performed by the HIL model. The measured loads are cleansed from the incorrect inertial and gravitational components and the estimated pure aerodynamic forces and torques are fed into the dynamic simulator, which numerically accounts for the true inertial and gravitational effects on the turbine together with the floater ones. In this work, it is not possible to apply a force correction a posteriori, as in Taruffi et al. (2024b), where the forces were corrected as a post-processing step because of the uncoupled nature of the prescribed motions. Here, the dynamics is fully-coupled and the measured loads are utilized in real-time to solve the floating motion. Thus, the correction has to be done in real-time. The aerodynamic forces and torques are estimated as:

$$F_{aero} = F_{meas} - F_{corr}, \quad T_{aero} = T_{meas} - T_{corr}, \tag{1}$$

$$F_{corr} = F_{in} + F_{grav}, \quad T_{corr} = T_{in} + T_{grav}, \tag{2}$$

where F_{aero} and T_{aero} are the estimated aerodynamic forces and torques, F_{meas} and T_{meas} are the forces and torques measured by the load cell placed under the nacelle, F_{corr} and T_{corr} are the correction forces and torques, F_{in} and T_{in} are the inertia forces and torques and F_{grav} and T_{grav} are the gravitational forces and torques. The forces and torques have three components each (x, y and z). Thus to obtain the aerodynamic forces, the inertial and gravitational forces that the load cell is measuring have to be estimated. This is done by relying on the acceleration measurements performed at the nacelle as follows:

$$F_{in} + F_{grav} = -Ma_{meas}, \quad T_{in} + T_{grav} = -R^{-1}\begin{bmatrix} J_x\ddot{\theta}_x \\ J_y\ddot{\theta}_y \\ J_z\ddot{\theta}_z \end{bmatrix} - \begin{bmatrix} Ma_{meas}(y)z_{lc} \\ Ma_{meas}(x)z_{lc} \\ 0 \end{bmatrix}, \tag{3}$$

where M is the mass of the scale model rotor-nacelle assembly, J is the moment of inertia, a_{meas} is the translational acceleration measured by the triaxial accelerometer placed at the nacelle, R is the rotation matrix (see Section A2) and z_{lc} is the vertical distance between the center of mass and the load cell sensor. The angular accelerations $\ddot{\theta}_x$, $\ddot{\theta}_y$ and $\ddot{\theta}_z$ are neglected because of the lack of a reliable source for these values in real-time. An angular acceleration sensor is not used in the current setup. Additionally, deriving the accelerations from the angular position feedback from the hexapod resulted in another error with respect to negation due to the derivation operation and the delays between sensors signals and hexapod feedback. As proved in Section 3.3.2, this has a visible effect only in the yaw degree-of-freedom. In roll and pitch, the term Ma_{meas} is larger, and therefore, the omission does not lead to noticeable errors. To minimize the de-synchronization of signals and delays, which harm the real-time character of the correction, no filter is applied to the force and acceleration inputs.

The value of M is estimated at 1.6kg via system identification by actuating known motions and reading inertia forces with the same load cell as in the tests. This reduces errors in the force correction that could arise from using a different sensor. After correction, the aerodynamic forces are transformed from the rotating reference frame centered at the nacelle to the non-rotating reference frame centered at the FOWT still water level (SWL).

https://doi.org/10.5194/wes-2025-100
Preprint. Discussion started: 30 June 2025

WIND ENERGY SCIENCE DISCUSSIONS

3.2 Floater dynamics

A numerical model is developed to simulate the floater dynamics. This model takes as input the estimated aerodynamic forces and computes the motion response of the FOWT in six degrees-of-freedom returning as output the position to be imposed on the hexapod. A compromise between fidelity and computational cost has to be made to ensure the capability of running the model in real-time. Thus the modelling follows a mid-fidelity approach, similar to the widely-used simulation tool FAST (Jonkman and Buhl, 2005) and previous HIL setups (Belloli et al., 2020). The focus of this setup is on the motion-induced aerodynamic loads and the floater dynamics have to be reproduced sufficiently accurately to produce realistic motions, by which the aerodynamics are affected. The focus of this study is not on analysing the details hydrodynamics or mooring effects. For this reason, a higher-fidelity hydrodynamic model (e.g. computational fluid dynamics) is out of scope and not feasible given the real-time constraints.

The motion response - in physics-based models - is determined by solving the equations of motion. For FOWTs, this is commonly done with a derived version of the Cummins equation (Cummins et al., 1962), which models the complete dynamics of the floater as a damped spring-mass system subjected to external forces, such as aerodynamics, hydrodynamics, and mooring forces. The model used here is flexibly targeted at semi-submersible floaters supporting wind turbines in the 10MW size range. The general equation of motion solved, and the specific choices made here, are presented hereafter. The equations of motion are given by:

$$(M+A)\ddot{x} + R\dot{x} + R_2\dot{x}^2 + Kx = F_{\text{hydro}} + F_{\text{moor}} + F_{\text{aero}}, \tag{4}$$

where M is the structural mass, A is the added mass, R is the linear viscous damping, R_2 is the quadratic damping (here not modelled), and K is the total stiffness. All are 6×6 matrices. The external 6×1 force vectors are: F_{hydro} for the hydrodynamic force, F_{moor} for the mooring load (here not modelled), and F_{aero} for the aerodynamic force. Additionally, x is the position coordinates vector, $\dot{x}$ is the velocity vector, and $\ddot{x}$ is the acceleration vector. The stiffness terms include the gravitational (K_{grav}), the mooring (K_{moor}) and the hydrostatic contributions (K_{hst}). The viscous effects are approximated as linear and quadratic (for some floaters) global viscous damping matrices. A comprehensive equation of motion is detailed in Appendix A4.

The hydrostatic and hydrodynamics are modelled using the potential flow theory. The effects considered are hydrostatic restoring, radiation damping and first-order incident wave diffraction. Their calculation relies on panel code (e.g. WAMIT) simulation outputs representing the floater's hydro-properties. The hydrostatic restoring contribution is accounted for in the stiffness matrix of the system. The first-order diffraction forces are pre-calculated based on the sea state corresponding to the test case and use the JONSWAP spectrum for irregular waves with WAFO tool (Brodtkorb et al., 2000). The radiation forces instead need to be calculated in real-time. Normally, a convolution integral needs to be computed to keep the memory effect. Given the real-time application, a state-space approximation is preferred. The state-space model parameters are identified using a state-space identification tool (SS_Fitting) developed by Duarte et al. (2013). The infinite-frequency added mass is the term A while its frequency-dependant part is accounted for in the radiation calculation.

https://doi.org/10.5194/wes-2025-100
Preprint. Discussion started: 30 June 2025

A linear approach is used for the mooring lines in the form of a stiffness matrix. As detailed in 3.3.1, the model is then tuned with FAST as benchmark.

The properties of the selected concept relevant to building the dynamic model are in Table 2 and are obtained from Lemmer et al. (2016) and Lemmer et al. (2020), where the hydro-properties are available.

3.3 HIL assessment

Prior to wind tunnel testing, it is of utmost importance to assess the HIL setup, to ensure the trustworthiness of the results. Both the dynamic model and the HIL architecture itself, namely the measurement and actuation loop and the force correction method, must be verified. This is done following a methodology that can be considered a best practice for hardware-in-the-loop wind tunnel testing and covers 3 steps of assessment and measurements:

1. Tuning and verification of the dynamic model
2. Verification of the *loop*
3. Aerodynamic measurements

3.3.1 Floater simulator

Step 1 is to verify the dynamic model simulating the floater. This is done by performing standalone simulations in Simulink and it corresponds to testing in *Open-Loop*, i.e. without force feedback. It is to assess the modelling of the FOWT rigid body dynamics, hydrodynamic and mooring. FAST is used as benchmark for comparison. In this step only, the simulations are performed at full-scale.

The rigid-body dynamics are determined with free decay simulations individually for each degree-of-freedom. Free decays are commonly used to characterize the rigid-body dynamics of floating systems, from which the natural frequency and linear damping ratio are evaluated. The wave response is evaluated with simulations in wave conditions. The simulations, both in Simulink and FAST, are always run with no wind and no rotation of the rotor. The mooring is simulated dynamically in FAST using MoorDyn module, while linearly in Simulink.

The dynamic model is fine-tuned adjusting the damping and stiffness term to match the FAST simulations. This tuning process is done iteratively and for each degree-of-freedom. Small initial conditions ($2\mathrm{m}$ for translational DOFs and $2\mathrm{deg}$ for rotational DOFs) are used to stay within a fairly linear range in the mooring reproduction in the benchmark.

The comparison between the decays for each DOF can be seen in the time domain in Fig. 4, where the tuned dynamic model closely resembles the response of FAST, and the obtained values of natural frequency and damping ratio are reported in Table 4. Overall, the decay responses match satisfactorily.

https://doi.org/10.5194/wes-2025-100
Preprint. Discussion started: 30 June 2025

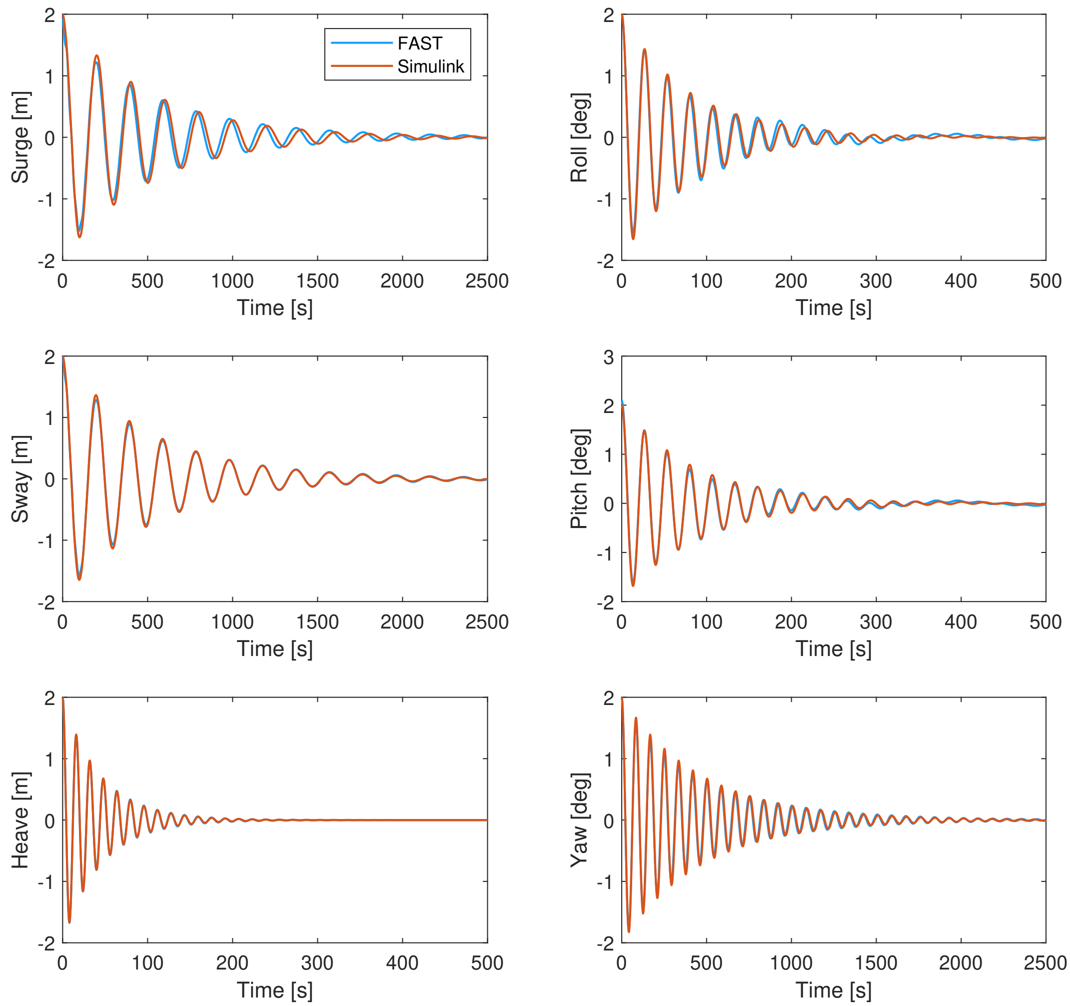

Figure 4. Time histories of floater DOFs for decay simulations with FAST (benchmark) and with the standalone HIL numerical model. Simulations are performed and visualised at full-scale.

3.3.2 HIL setup

With the verified dynamic model, step 2 is to assess the HIL architecture itself and specifically the force-feedback and motion-actuation chain with the force correction procedure. To assess it, it is necessary to isolate its effect. This is done by testing in *Closed-Loop* - with the force feedback activated - and comparing the same case tested in *Open-Loop* - simulation without force input. Free decay cases in each degree-of-freedom are performed in no-wind and no-rotation conditions so that the only difference with the open-loop tests is the activation of the force feedback. Since there is virtually no aerodynamic force involved, neglecting the non-rotating rotor drag, ideally the motion response in *Closed-Loop* should exactly match the *Open-Loop*. This implies that the *loop* and the force correction work correctly and all the rotor non-aerodynamic loads, which are undesired inertia and gravitational forces measured by the load cell in the closed-loop configuration only, are cancelled out

https://doi.org/10.5194/wes-2025-100
Preprint. Discussion started: 30 June 2025

correctly. An incomplete or wrong correction would result in a different motion response, for example, an amplification or a change in natural frequency and damping.

The comparison is shown in time and frequency domain in Fig. 5 and Fig. 6 respectively, and Table 4 reports natural frequency and damping values. The open-loop and closed-loop tests match closely with the only exception of the yaw case. This is attributed to the substantial lack of force correction in this DOF with the absence of a reliable source for yaw acceleration. This, as explained in Section 3.1, is not happening in the other rotational DOFs because the inertial effect due to the rotation is small compared to the total inertial effect (i.e. translational acceleration with an offset centre of gravity with respect to the load cell) and a non-correction of the first produces negligible effects. Moreover, this study does not focus on asymmetrical cases such as misaligned wind and waves and, for this reason, this error has a limited impact. Overall, this match assesses the HIL system and ensures the results obtained in the wind tests are accurate.

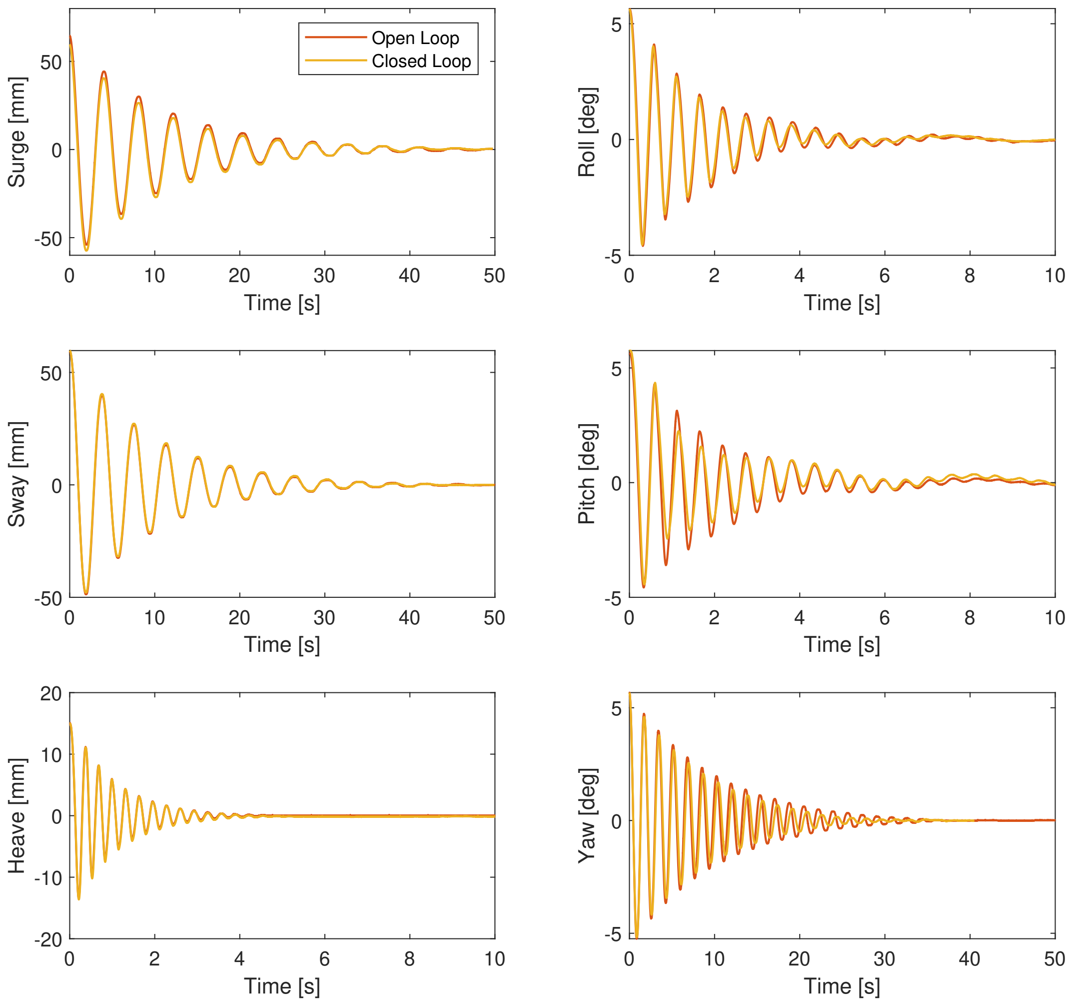

Figure 5. Time histories of floater DOFs for decay tests with the HIL setup in *Open-Loop* and *Closed-Loop* configuration. The results are at model-scale.

https://doi.org/10.5194/wes-2025-100
Preprint. Discussion started: 30 June 2025

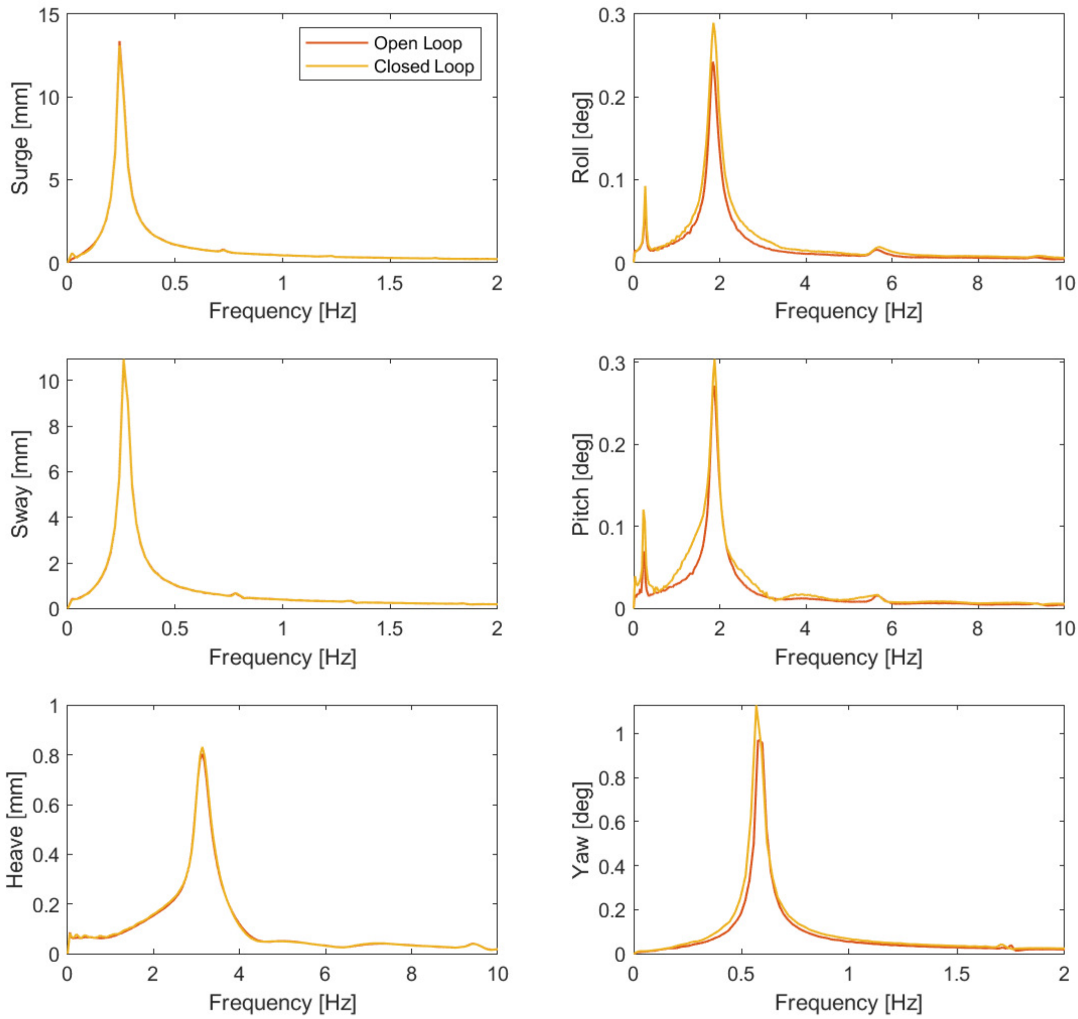

Figure 6. Frequency spectra of floater DOFs for decay tests with the HIL setup in *Open-Loop* and *Closed-Loop* configuration. The results are at model-scale.

3.3.3 Real-time limitations

Keeping the real-time in the floater simulation and ensuring latencies within a limit are of fundamental importance. The real-time machine integrates the HIL model with a time step of $1\mathrm{ms}$. The force and acceleration sensors show no visible lag between their signals. This eases the force correction process, as a lag could cause a mis-correction. The sensors are used within their
305 response range, i.e. $0-200\mathrm{Hz}$ for the accelerometer and sensibly higher for the force sensor. The actuation latency of the

https://doi.org/10.5194/wes-2025-100
Preprint. Discussion started: 30 June 2025

hexapod was estimated considering the delay between the position command from the real-time machine to the hexapod and the position feedback from the hexapod to the real-time machine, and the latency between the command and actual motion was assumed to be half of it. The total latency between the physical phenomena, i.e. the aerodynamic loads acting on the rotor, and the motion that it induces is estimated as about $50\mathrm{ms}$.

4 Aerodynamic response

After assessment of the HIL setup, aerodynamic measurements can be performed with wind tunnel tests as step 3. This work has its focus on the HIL setup development and assessment, thus a limited amount of tests and analyses are carried out. The aim is to explore the potential of the HIL setup of investigating the aerodynamic response of FOWTs. Decay tests are run to experimentally estimate the aerodynamic damping of the rotor and a set of realistic combined wind and wave cases are tested to study the wind and turbine effects on the floater motion response. The aerodynamic tests are performed in wind conditions and with the turbine rotor spinning at a fixed speed. The HIL feedback system is always active (*Closed-Loop*).

4.1 Aerodynamic damping

With HIL, the floater motion is not pre-calculated but computed in real-time based on the measured aerodynamic loads. Thus, it is straightforward to quantify the effect of the rotor aerodynamic damping on the floater motion response and estimate the aerodynamic damping itself. This is achieved by performing *Closed-Loop* decay tests in wind conditions for each DOF and comparing the results with no-wind decays. From the comparison, the effect of the rotor aerodynamics can be investigated and the aerodynamic damping can be quantitatively estimated. These cases are performed with the turbine operating at rated conditions.

The time domain comparison is shown in Fig. 7 and a frequency domain analysis is in Fig. 8. From the later, the natural frequency of each DOF is visible as the highest peak. Before the peak of the natural frequency, there is another peak visible in roll and pitch. This smaller peak is the natural frequency of sway and surge, respectively. This peak is visible due to the coupling between roll and sway, and pitch and surge. The smaller peak around 8Hz in heave and roll is the 1P frequency of the rotor, visible only in these DOFs.

The spectra with wind show peaks that are lower and broader for surge, pitch and yaw degrees of freedom. This implies that the rotor provides damping. The thrust force acting on the rotor has a damping effect on the motion in these DOFs for the motions that have components in the direction of thrust. Assuming no control is present as in the tests, the rotor moving against the wind direction in surge or pitch motions results in an increase of thrust force due to the increase in relative wind speed seen by the rotor. When the rotor is moving in the direction of the wind, the thrust force decreases for the same reason. The increase and decrease in thrust force oppose the motion, slowing down the oscillation with a damping effect. A similar phenomenon explains the damping in yaw oscillation, where the part of the rotor that moves against the wind sees an increase in relative speed and consequently of force in the wind direction which opposes the motion. The opposite happens simultaneously on the other side, causing the damping effect. A quantitative analysis is done to estimate the aerodynamic damping effect on DOFs

https://doi.org/10.5194/wes-2025-100
Preprint. Discussion started: 30 June 2025

natural frequencies and damping, repeating the decay tests for three initial conditions, and the results are reported in Table 4. The pitch DOF is the most largely affected, showing an average increase in the damping of 220% in rated wind compared to
340 no-wind. This is followed by yaw with 52% increase and surge with 19%.

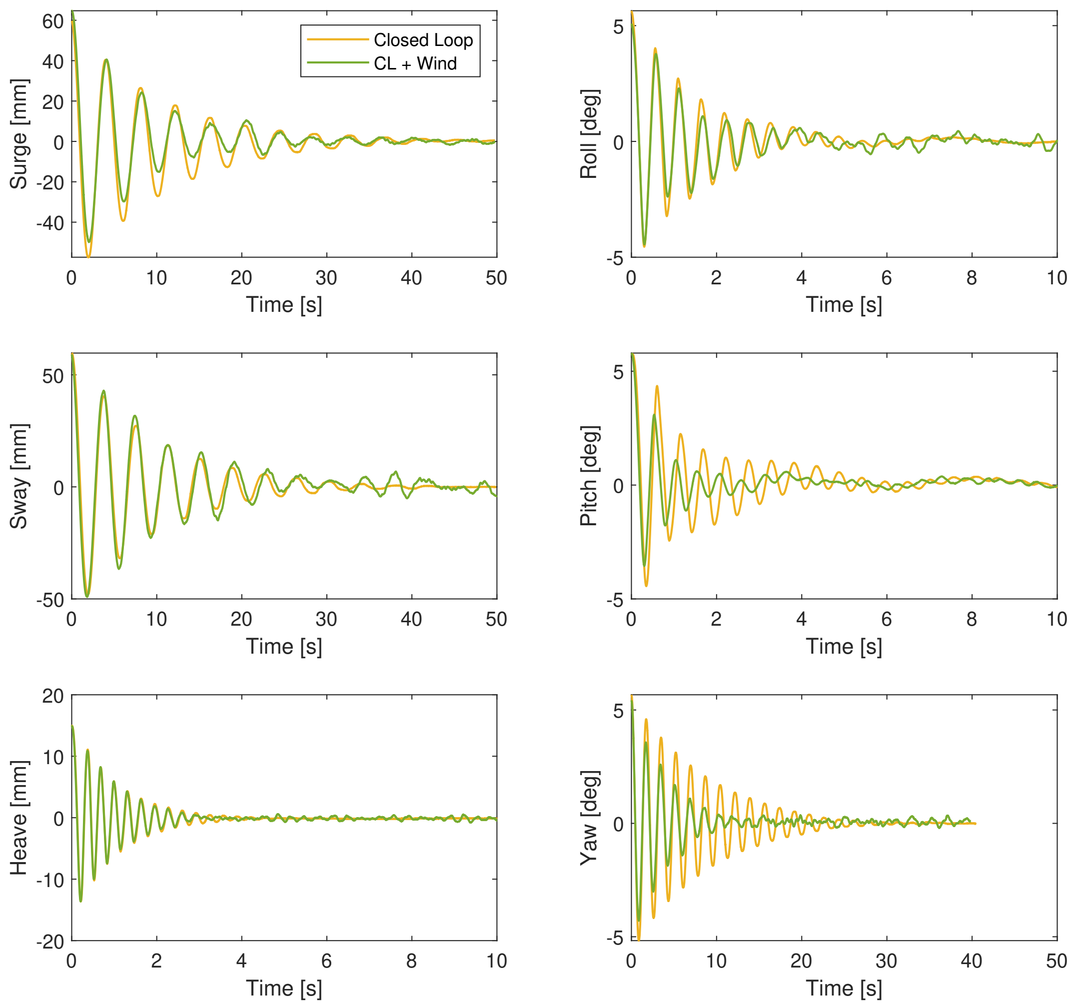

Figure 7. Time histories of floater DOFs for HIL (*Closed-Loop*) decay tests in *no-Wind* and *Wind* conditions. The results are at model-scale.

https://doi.org/10.5194/wes-2025-100
Preprint. Discussion started: 30 June 2025

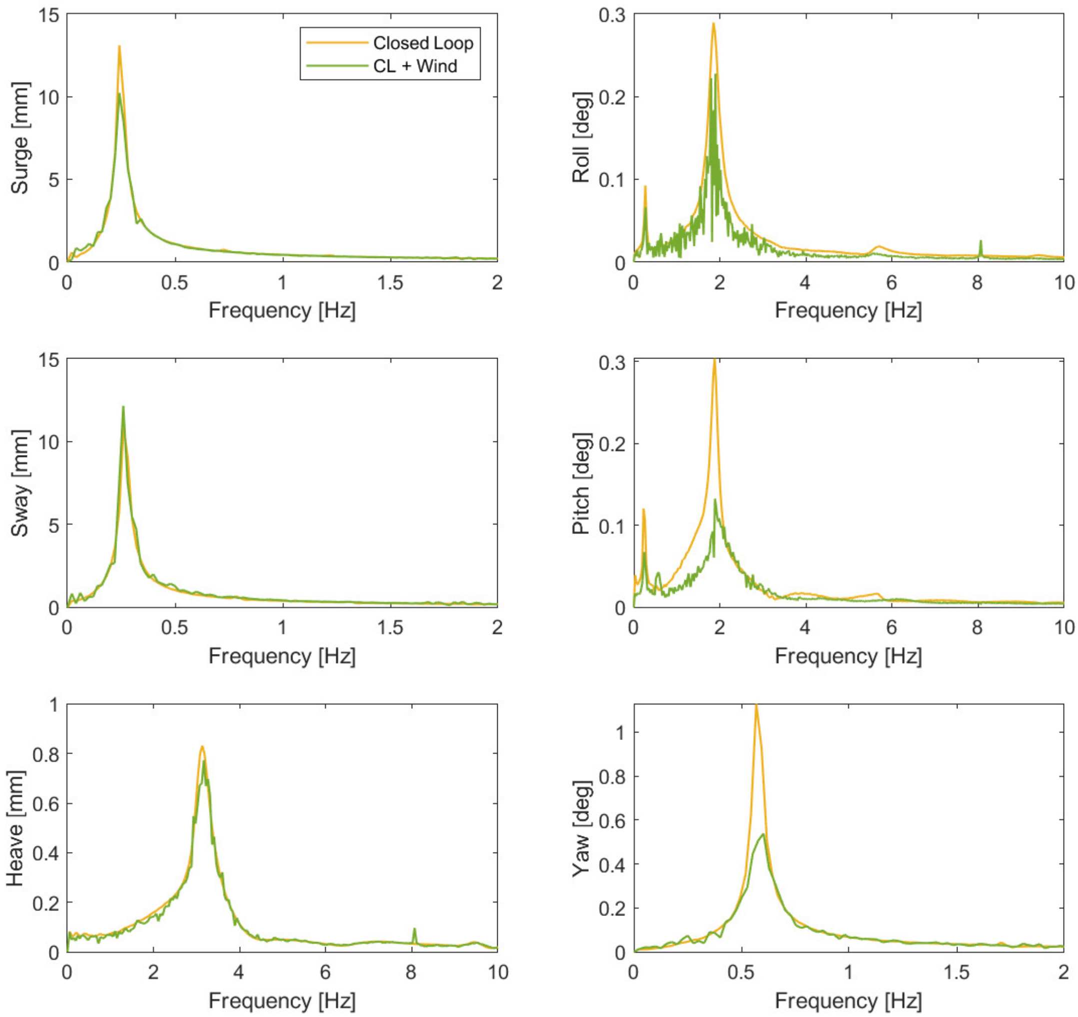

Figure 8. Frequency spectra of floater DOFs for HIL (*Closed-Loop*) decay tests in *no-Wind* and *Wind* conditions. The results are at model-scale.

https://doi.org/10.5194/wes-2025-100
Preprint. Discussion started: 30 June 2025

eawe european academy of wind energy
Open Access WIND ENERGY SCIENCE DISCUSSIONS

Table 4. Natural frequencies and damping ratios of the floater DOFs obtained from decay cases with FAST, with the HIL model and in the HIL tests in *Closed-Loop* and *Closed-Loop & Wind* configurations. The values of *Closed-Loop* and *Closed-Loop & Wind* are averaged over three different initial conditions and are upscaled to full-scale for the comparison. The last column shows the effect of aerodynamic damping in wind-aligned DOFs.

	FAST		HIL Model		Closed-Loop		Closed-Loop & Wind		
DOF	Nat. Freq. [Hz]	Damp. [-]	Nat. Freq. [Hz]	Damp. [-]	Nat. Freq. [Hz]	Damp. [-]	Nat. Freq.[Hz]	Damp. [-]	Aero. Damp. [%]
Surge	0.0050	0.056	0.0050	0.062	0.0050	0.069	0.0051	0.082	+ 19
Sway	0.0051	0.057	0.0051	0.059	0.0054	0.066	0.0054	0.043	
Heave	0.063	0.058	0.063	0.058	0.065	0.051	0.065	0.043	
Roll	0.038	0.059	0.037	0.054	0.037	0.059	0.037	0.074	
Pitch	0.038	0.059	0.037	0.050	0.038	0.047	0.040	0.15	+ 210
Yaw	0.012	0.032	0.012	0.029	0.012	0.035	0.012	0.054	+ 52

4.2 Wind and wave tests

Combined wind and wave cases were tested to demonstrate that the setup is suitable for reproducing realistic loading conditions. Five irregular wave sea states are tested in total, each with a corresponding wind condition. The selected cases (see Table 5) are in the normal operational range of the FOWT as representative of a deployment site with a moderate sea state. They are limited to the capability of the setup as the harshest waves cannot be tested because the motion response would go beyond what the Hexapod allows in terms of accelerations. Also, the wind speed is capped to the rated value since the wind turbine model cannot operate at above-rated conditions due to the absence of blade-pitch actuation.

Table 5. Load cases for combined wind and wave conditions. The operational irregular waves are from (Krieger et al., 2015) and the corresponding uniform wind speed is capped to rated. All parameters are at full-scale.

Case	Wave sign. height [m]	Wave peak period [s]	Wind speed [m/s]	Rotor speed [rpm]
1	1.38	7	7	6
2	1.67	8	7.1	6.04
3	2.2	8	10.3	8.27
4	3.04	9.5	11.4	9.6
5	4.29	10	11.4	9.6

From the motion response spectra in Fig. 9 for an illustrative operational wind and wave case with wind speed at the rated value (case 4), it is visible that there are two significant areas of activity. The first is near the natural frequency range of the floating platform, which is towards the lower frequency range; this is also the region where the effects of wind are visible. The second is near the wave frequency range, where the activity due to the emulated wave can be observed, the frequency of the highest energy wave is denoted with a dashed line. The responses in the surge, pitch and heave DOFs are more pronounced in this region, this is expected since the wave heading in these test cases is set at $0\deg$. Finally, the rotor frequency (i.e. 1P frequency), denoted with the dotted line, shows a significant response in the heave and the roll DOFs compared to other regions

https://doi.org/10.5194/wes-2025-100
Preprint. Discussion started: 30 June 2025

of activity and response is present in this frequency in all DOFs. The dynamic response to wind and waves is qualitatively in line with what was expected from literature, confirming the suitability of the setup for this kind of study.

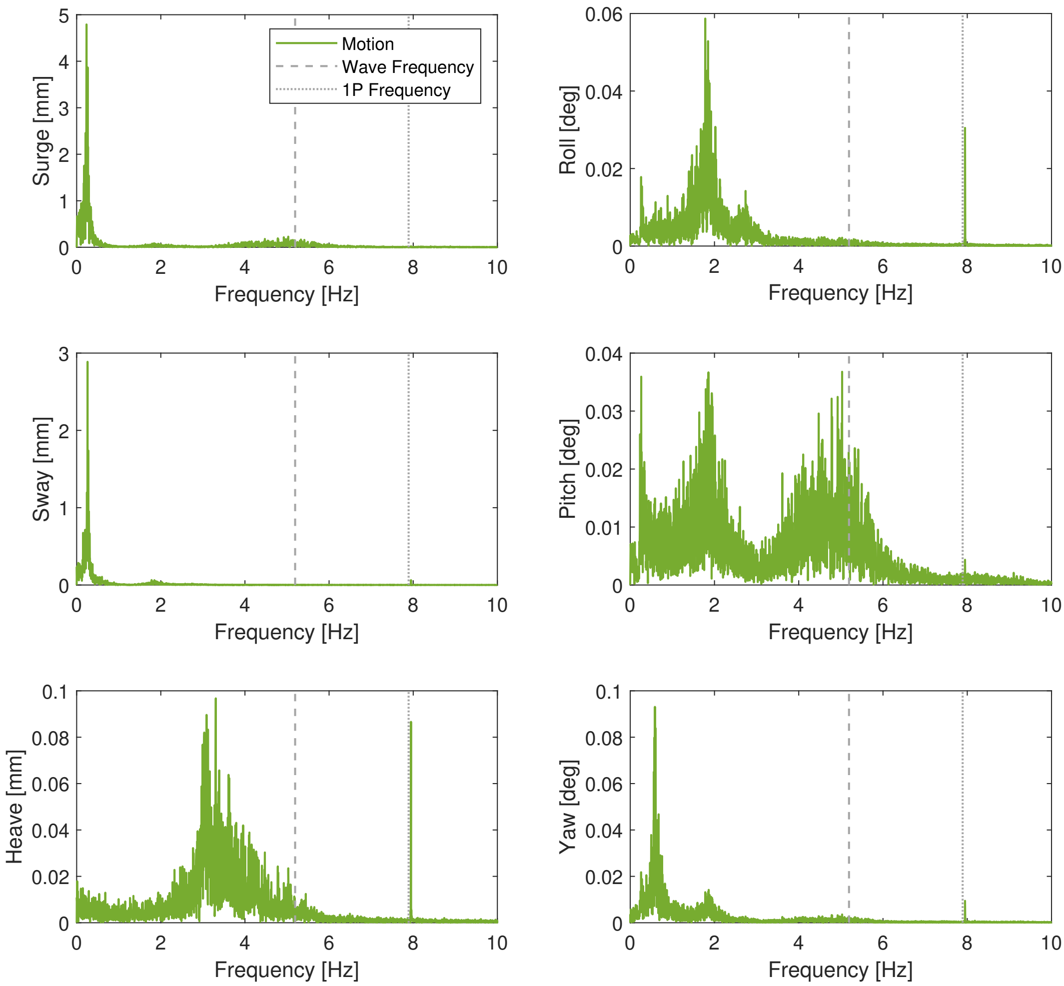

Figure 9. Frequency spectra of floater motion response to the combined wind (HIL in *Closed-Loop* configuration) and wave loading. The results are at model-scale.

5 Conclusions

This work presents a hardware-in-the-loop (HIL) wind tunnel setup designed to study the coupled aerodynamic and motion response of floating offshore wind turbines (FOWTs). At the time of writing, only one other wind tunnel HIL setup (Belloli et al., 2020) exists for this purpose and only few experiments have been carried out with the full dynamic coupling. There is thus a need to develop more complementary setups for comparison and further investigations.

https://doi.org/10.5194/wes-2025-100
Preprint. Discussion started: 30 June 2025

WIND ENERGY SCIENCE DISCUSSIONS

Unlike prescribed motion tests, which pre-calculate floating motions without accounting for the mutual interaction between aerodynamic forces and motion response, the HIL approach closes the loop and captures the two-way interactions. The aerodynamic loads influence the motion, and in turn, the motion affects the aerodynamic loads. By including the aerodynamic feedback in real-time, the setup provides a true reproduction of FOWT dynamics, enabling studies, such as the estimation of the aerodynamic damping, that cannot be obtained from uncoupled approaches. Investigating the effect of aerodynamic damping on the motion response with a scaled rotor is therefore rare in the literature.

A key novelty of this work is the development and application of a new force correction methodology. By measuring forces at the tower top, the approach significantly improves the accuracy of aerodynamic load estimation, minimizing the inertia-to-aerodynamic force ratio. Compared to a previous method that relied on tower-base measurements, this approach reduces the compounding effects of inertial and gravitation forces, ensuring that the aerodynamic response is more accurate.

The setup hardware already proved capable of operating across the dynamic range relevant to FOWTs, necessary for triggering unsteady aerodynamic phenomena (Taruffi et al., 2024b). Here, with the addition of the HIL, it demonstrated its ability to replicate accurate aerodynamic-driven motion responses. The versatility of this setup makes it a powerful tool for studies with different FOWT configurations. The floater numerical model and the reference-scaled rotor allow for flexibility in simulating different turbine and floater concepts, and the validated coupling architecture ensures accurate representation of aerodynamic phenomena.

A preliminary study highlights the significant impact of aerodynamics on the rigid-body dynamics of FOWTs, particularly in surge and pitch degrees of freedom. Measurable effects are also shown in yaw, however results may be impaired by an imperfect force correction in that DOF.

In conclusion, this work introduces a scalable, assessed, and versatile experimental framework for FOWT aerodynamic studies. Future studies will build on these results, extending the methodology to address remaining challenges and exploring the aerodynamic behaviour of new turbine designs under increasingly realistic conditions.

Appendix A: Analytical formulations

A1 Force correction

As integration to Section 3.1, a more complete analytical formulation of the force correction methodology used in the HIL model is illustrated in this appendix. This is to explain the theory behind the formulation in Eq. 3.

https://doi.org/10.5194/wes-2025-100
Preprint. Discussion started: 30 June 2025

The forces and torques measured by the load cell installed under the nacelle can be analytically expressed as:

$$F_{meas} = \underbrace{\begin{bmatrix} F_{aero,x} \\ F_{aero,y} \\ F_{aero,z} \end{bmatrix}}_{F_{aero}} + R^{-1} \left(+ \underbrace{\begin{bmatrix} 0 \\ 0 \\ -M_{rna} g \end{bmatrix}}_{F_{grav}} - \underbrace{\begin{bmatrix} M\ddot{x} \\ M\ddot{y} \\ M\ddot{z} \end{bmatrix}}_{F_{in,trans}} - M \underbrace{\left(\begin{bmatrix} \ddot{\phi} \\ \ddot{\theta} \\ \ddot{\psi} \end{bmatrix} \times \left(R \begin{bmatrix} 0 \\ 0 \\ hh \end{bmatrix} \right) \right)}_{F_{in,tang}} - M \underbrace{\left(\begin{bmatrix} \dot{\theta}_x \\ \dot{\theta}_y \\ \dot{\theta}_z \end{bmatrix} \times \left(\begin{bmatrix} \dot{\theta}_x \\ \dot{\theta}_y \\ \dot{\theta}_z \end{bmatrix} \times \overbrace{\left(R \begin{bmatrix} 0 \\ 0 \\ h \end{bmatrix} \right)}^{pos_{tt}} \right) \right)}_{F_{in,centr}} \right), \tag{A1}$$

and:

$$T_{meas} = \underbrace{\begin{bmatrix} T_{aero,x} \\ T_{aero,y} \\ T_{aero,z} \end{bmatrix}}_{T_{aero}} - R^{-1} \underbrace{\begin{bmatrix} J_x\ddot{\theta}_x \\ J_y\ddot{\theta}_y \\ J_z\ddot{\theta}_z \end{bmatrix}}_{T_{in,rot}} + \underbrace{\begin{bmatrix} F^*_{in,x} z_{lc} \\ F^*_{in,y} z_{lc} \\ 0 \end{bmatrix}}_{T_{in,trans}}, \tag{A2}$$

where:

- F_{meas} are the forces theoretically measured by the load cell
- T_{meas} are the torques theoretically measured by the load cell
- $F_{aero,x}$, $F_{aero,y}$, $F_{aero,z}$ are the aerodynamic forces
- $T_{aero,x}$, $T_{aero,y}$, $T_{aero,z}$ are the aerodynamic torques
- M_{rna} is the mass of the RNA
- J_{rna} is the inertia of the RNA
- g is the gravity acceleration
- R is the rotation matrix
- hh is the hub height
- z_{lc} is the distance between the RNA centre of mass and the load cell
- $\ddot{x}$, $\ddot{y}$, $\ddot{z}$ are the acceleration in surge, sway and heave (in the fixed frame, at tower bottom)
- $\ddot{\theta}_x$, $\ddot{\theta}_y$, $\ddot{\theta}_z$ are the rotational accelerations in roll, pitch and heave (in the fixed frame)
- * means: already calculated

https://doi.org/10.5194/wes-2025-100
Preprint. Discussion started: 30 June 2025

The accelerations measured by the accelerometer installed at the nacelle can be analytically expressed as:

$$a_{meas} = R^{-1} \cdot \left(\underbrace{-\begin{bmatrix} 0 \\ 0 \\ -g \end{bmatrix}}_{a_{grav}} + \underbrace{\begin{bmatrix} \ddot{x} \\ \ddot{y} \\ \ddot{z} \end{bmatrix}}_{a_{trans}} + \underbrace{\left(\begin{bmatrix} \ddot{\theta}_x \\ \ddot{\theta}_y \\ \ddot{\theta}_z \end{bmatrix} \times \left(R \begin{bmatrix} 0 \\ 0 \\ hh \end{bmatrix} \right) \right)}_{a_{tang}} + \underbrace{\left(\begin{bmatrix} \dot{\theta}_x \\ \dot{\theta}_y \\ \dot{\theta}_z \end{bmatrix} \times \left(\begin{bmatrix} \dot{\theta}_x \\ \dot{\theta}_y \\ \dot{\theta}_z \end{bmatrix} \times \left(R \begin{bmatrix} 0 \\ 0 \\ hh \end{bmatrix} \right) \right) \right)}_{a_{centr}} \right), \tag{A3}$$

where:

- a_{meas} are the accelerations theoretically measured by the accelerometer
- g is the gravity acceleration
- R is the rotation matrix
- hh is the hub height
- $\ddot{x}$, $\ddot{y}$, $\ddot{z}$ are the acceleration in surge, sway and heave (in the fixed frame, at tower bottom)
- $\ddot{\theta}_x$, $\ddot{\theta}_y$, $\ddot{\theta}_z$ are the rotational accelerations in roll, pitch and heave (in the fixed frame)

The formulation of the force correction in 3 is obtained from here.

A2 Rotation matrices

Rotation transformation matrices are used in the HIL model. This is necessary because the equation of motion is solved in the fixed frame, while the acceleration and force measurements are taken by sensors attached to the wind turbine, which are in a rotating frame. The rotation matrices are first determined to transform from the rotating frame to the fixed frame. The rotation matrices are:

Yaw Rotation:

$$R_z(\psi) = \begin{bmatrix} \cos(\psi) & -\sin(\psi) & 0 \\ 3\sin(\psi) & \cos(\psi) & 0 \\ 0 & 0 & 1 \end{bmatrix}$$

Pitch Rotation:

$$R_y(\theta) = \begin{bmatrix} \cos(\theta) & 0 & \sin(\theta) \\ 0 & 1 & 0 \\ -\sin(\theta) & 0 & \cos(\theta) \end{bmatrix}$$

https://doi.org/10.5194/wes-2025-100
Preprint. Discussion started: 30 June 2025

eawe european academy of wind energy
Open Access WIND ENERGY SCIENCE DISCUSSIONS

Roll Rotation:

$$R_x(\phi) = \begin{bmatrix} 1 & 0 & 0 \\ 0 & \cos(\phi) & -\sin(\phi) \\ 0 & \sin(\phi) & \cos(\phi) \end{bmatrix}$$

The order of rotations, or the Euler sequence, plays a crucial role in the transformation matrix, as different sequences can yield different results. For a 6DOF system, the transformation matrices are multiplied threefold, so the rotation order must be set correctly to avoid amplifying errors. The generally accepted order of rotation is the Yaw-Pitch-Roll transformation. When applying this transformation, the matrices are multiplied in the Roll-Pitch-Yaw order. The final rotation matrix is:

$$R = R_z(\psi)R_y(\theta)R_x(\phi) \tag{A4}$$

This order of rotation is used to transform from a rotating reference frame to a fixed reference frame. The inverse of the transformation is used to convert from a fixed frame to a rotating frame.

A3 Force rotation and transport

The forces have to be transformed from the rotating frame they are measured into a fixed frame. The equation of motion is solved at the MSL (mean sea level), i.e. at the tower base. Hence, the transportation of the forces to the tower base is also necessary. The aerodynamic force and torque used in the equation of motion ($F_{aero,tb}, T_{aero,tb}$, where tb stands for tower-bottom) are:

$$F_{aero,tb} = R \cdot F_{aero} \tag{A5}$$

$$T_{aero,tb} = \begin{bmatrix} F_{aero,f}(x) \\ -F_{aero,f}(y) \\ F_{aero,f}(z) \end{bmatrix} \times \begin{bmatrix} pos_{tt}(x) \\ -pos_{tt}(y) \\ pos_{tt}(z) \end{bmatrix} + T_{aero} \tag{A6}$$

A4 Equation of motion

A complete formulation of the equation of motion of the rigid body dynamics of FOWTs is shown here to complement Eq. 4:

$$(M_\mathrm{s} + A)\ddot{x} + R_\mathrm{visc}\dot{x} + R_{2,\mathrm{visc}}\dot{x}^2 + K_\mathrm{grav} + K_\mathrm{hst} + F_\mathrm{moor}x = F_\mathrm{rad} + F_{\mathrm{diff},1} + F_\mathrm{moor} + F_{\mathrm{aero,\,est.}}, \tag{A7}$$

where:

- M_s is the structural mass and inertia matrix of the whole FOWT (rotor included)
- A is the infinite-frequency hydrodynamic added mass
- R_visc is the linear viscous hydrodynamic damping matrix

https://doi.org/10.5194/wes-2025-100
Preprint. Discussion started: 30 June 2025

- $R_{2,\text{visc}}$ is the quadratic viscous hydrodynamic damping matrix
- K_{grav} is the gravitational restoring stiffness matrix of the entire FOWT (rotor included)
- K_{hst} is the hydrostatic restoring stiffness matrix
- K_{moor} is the linearized mooring stiffness matrix
- F_{rad} is the calculated radiation force (with state-space approximation)
- $F_{\text{diff},1}$ is the generated first order diffraction force
- $F_{\text{diff},2}$ is the generated second order diffraction force
- F_{moor} is the calculated mooring force
- $F_{\text{aero, est.}}$ is the aerodynamic force estimated from the measures

Data availability. The dataset is accessible upon request to the authors.

Author contributions. FT and AV imagined the scope of the work and designed the experimental campaign. FT developed the experimental setup. FT and ST developed the numerical models and carried out the tests. ST performed the analyses of the results. FT and ST performed the literature review. FT prepared the manuscript including contributions from the co-authors and the interpretation of the results. AV was responsible for the supervision and the manuscript revisions.

Competing interests. The authors declare that they have no conflict of interest.

Acknowledgements. The research is partially funded by the Dutch National Research Council (NWO) within the project HybridLabs (NWA.1518.22.066) of the research programme Dutch Research Agenda – research along NWA routes by consortia and through the Talent Programme Vidi scheme (project number 19675).

https://doi.org/10.5194/wes-2025-100
Preprint. Discussion started: 30 June 2025

References

Armesto, J. A., Jurado, A., Guanche, R., Couñago, B., Urbano, J., and Serna, J.: TELWIND: Numerical Analysis of a Floating Wind Turbine Supported by a Two Bodies Platform, in: Volume 10: Ocean Renewable Energy, American Society of Mechanical Engineers, ISBN 978-0-7918-5131-9, https://doi.org/10.1115/OMAE2018-77587, 2018.

Azcona, J., Bouchotrouch, F., González, M., Garciandía, J., Munduate, X., Kelberlau, F., and Nygaard, T. A.: Aerodynamic Thrust Modelling in Wave Tank Tests of Offshore Floating Wind Turbines Using a Ducted Fan, Journal of Physics: Conference Series, 524, 012 089, https://doi.org/10.1088/1742-6596/524/1/012089, 2014.

Azcona, J., Bouchotrouch, F., and Vittori, F.: Low-frequency dynamics of a floating wind turbine in wave tank–scaled experiments with SiL hybrid method, Wind Energy, 22, 1402–1413, https://doi.org/10.1002/we.2377, 2019.

Bachynski, E. E., Thys, M., Sauder, T., Chabaud, V., and Sæther, L. O.: Real-Time Hybrid Model Testing of a Braceless Semi-Submersible Wind Turbine: Part II — Experimental Results, in: Volume 6: Ocean Space Utilization; Ocean Renewable Energy, American Society of Mechanical Engineers, ISBN 978-0-7918-4997-2, https://doi.org/10.1115/OMAE2016-54437, 2016.

Bak, C., Zahle, F., Bitsche, R., Kim, T., Yde, A., Henriksen, L. C., Nata-rajan, A., and Hansen, M. H.: Department of Wind Energy I-Report Description of the DTU 10 MW Reference Wind Turbine, 2013.

Bayati, I., Belloli, M., Bernini, L., and Zasso, A.: Wind Tunnel Wake Measurements of Floating Offshore Wind Turbines, Energy Procedia, 137, 214–222, https://doi.org/10.1016/j.egypro.2017.10.375, 2017.

Bayati, I., Facchinetti, A., Fontanella, A., and Belloli, M.: 6-DoF hydrodynamic modelling for wind tunnel hybrid/HIL tests of FOWT: the real-time challenge, in: International Conference on Offshore Mechanics and Arctic Engineering, vol. 51319, p. V010T09A078, American Society of Mechanical Engineers, https://doi.org/10.1115/OMAE2018-77804, 2018a.

Bayati, I., Facchinetti, A., Fontanella, A., Giberti, H., and Belloli, M.: A wind tunnel/HIL setup for integrated tests of Floating Offshore Wind Turbines, Journal of Physics: Conference Series, 1037, 052 025, https://doi.org/10.1088/1742-6596/1037/5/052025, 2018b.

Belloli, M., Bayati, I., Facchinetti, A., Fontanella, A., Giberti, H., Mura, F. L., Taruffi, F., and Zasso, A.: A hybrid methodology for wind tunnel testing of floating offshore wind turbines, Ocean Engineering, 210, https://doi.org/10.1016/j.oceaneng.2020.107592, 2020.

Bredmose, H., Lemmer, F., Borg, M., Pegalajar-Jurado, A., Mikkelsen, R., Larsen, T. S., Fjelstrup, T., Yu, W., Lomholt, A., Boehm, L., and Armendariz, J. A.: The Triple Spar campaign: Model tests of a 10MW floating wind turbine with waves, wind and pitch control, Energy Procedia, 137, 58–76, https://doi.org/https://doi.org/10.1016/j.egypro.2017.10.334, 14th Deep Sea Offshore Wind RD Conference, EERA DeepWind'2017, 2017.

Brodtkorb, P. A., Johannesson, P., Lindgren, G., Rychlik, I., Rydén, J., and Sjö, E.: WAFO-a Matlab toolbox for analysis of random waves and loads, in: ISOPE International Ocean and Polar Engineering Conference, pp. ISOPE–I, isope, 2000.

Cermelli, C. and Aubault, A.: OTC 20674 Qualification of a Semi-Submersible Floating Foundation for Multi-Megawatt Wind Turbines, Tech. rep., http://onepetro.org/OTCONF/proceedings-pdf/10OTC/All-10OTC/OTC-20674-MS/1719099/otc-20674-ms.pdf/1, 2010.

Cummins, W. et al.: The impulse response function and ship motions, 1962.

Doisenbant, G., Boulluec, M. L., Scolan, Y.-M., and Guyot, M.: Application to reduced scale model testing, Wind Engineering, 42, 108–114, https://www.jstor.org/stable/90019972, 2018.

Duarte, T., Alves, M., Jonkman, J., and Sarmento, A.: State-Space Realization of the Wave-Radiation Force Within FAST, vol. Volume 8: Ocean Renewable Energy of *International Conference on Offshore Mechanics and Arctic Engineering*, p. V008T09A021, https://doi.org/10.1115/OMAE2013-10375, 2013.

https://doi.org/10.5194/wes-2025-100
Preprint. Discussion started: 30 June 2025

Fontanella, A., Da Pra, G., and Belloli, M.: Integrated Design and Experimental Validation of a Fixed-Pitch Rotor for Wind Tunnel Testing, Energies, 16, https://doi.org/10.3390/en16052205, 2023a.

Fontanella, A., Facchinetti, A., and Belloli, M.: Wind tunnel hardware-in-the-loop experiments about the global response of a 15 MW floating wind turbine, in: Journal of Physics: Conference Series, vol. 2626, Institute of Physics, ISSN 17426596, https://doi.org/10.1088/1742-6596/2626/1/012059, 2023b.

Goupee, A. J., Fowler, M. J., Kimball, R. W., Helder, J., and de Ridder, E.-J.: Additional Wind/Wave Basin Testing of the DeepCwind Semi-Submersible With a Performance-Matched Wind Turbine, in: Volume 9B: Ocean Renewable Energy, American Society of Mechanical Engineers, ISBN 978-0-7918-4554-7, https://doi.org/10.1115/OMAE2014-24172, 2014a.

Goupee, A. J., Koo, B. J., Kimball, R. W., Lambrakos, K. F., and Dagher, H. J.: Experimental comparison of three floating wind turbine concepts, Journal of Offshore Mechanics and Arctic Engineering, 136, https://doi.org/10.1115/1.4025804, 2014b.

Jonkman, J. M. and Buhl, M. L.: FAST User's Guide: Technical Report, 2005.

Krieger, A., Ramachandran, G. K. V., L., V., Gómez Alonso, P., González Almería, G., Berque, J., and Aguirre, G.: LIFES50+ D7.2: Design basis, 2015.

Lemmer, F., Amann, F., Raach, S., and Schlipf Swe, D.: Definition of the SWE-TripleSpar Floating Platform for the DTU 10MW Reference Wind Turbine, Tech. rep., 2016.

Lemmer, F., Raach, S., Schlipf, D., Faerron-Guzmán, R., and Cheng, P. W.: FAST model of the SWE-TripleSpar floating wind turbine platform for the DTU 10MW reference wind turbine, https://doi.org/10.18419/DARUS-514, 2020.

Oguz, E., Clelland, D., Day, A. H., Incecik, A., López, J. A., Sánchez, G., and Almeria, G. G.: Experimental and numerical analysis of a TLP floating offshore wind turbine, Ocean Engineering, 147, 591–605, https://doi.org/10.1016/j.oceaneng.2017.10.052, 2018.

Ramachandran, G., Vita, L., Krieger, A., and Mueller, K.: Design basis for the feasibility evaluation of four different floater designs, Energy Procedia, 137, 186–195, 2017.

Robertson, A. N., Jonkman, J. M., Goupee, A. J., Coulling, A. J., Prowell, I., Browning, J., Masciola, M. D., and Molta, P.: Summary of Conclusions and Recommendations Drawn From the DeepCwind Scaled Floating Offshore Wind System Test Campaign, vol. Volume 8: Ocean Renewable Energy of *International Conference on Offshore Mechanics and Arctic Engineering*, p. V008T09A053, https://doi.org/10.1115/OMAE2013-10817, 2013.

Rockel, S., Camp, E., Schmidt, J., Peinke, J., Cal, R., and Hölling, M.: Experimental Study on Influence of Pitch Motion on the Wake of a Floating Wind Turbine Model, Energies, 7, 1954–1985, https://doi.org/10.3390/en7041954, 2014.

Ruzzo, C., Muggiasca, S., Malara, G., Taruffi, F., Belloli, M., Collu, M., Li, L., Brizzi, G., and Arena, F.: Scaling strategies for multi-purpose floating structures physical modeling: state of art and new perspectives, Applied Ocean Research, 108, https://doi.org/10.1016/j.apor.2020.102487, 2021.

Schliffke, B., Aubrun, S., and Conan, B.: Wind Tunnel Study of a "Floating" Wind Turbine's Wake in an Atmospheric Boundary Layer with Imposed Characteristic Surge Motion, Journal of Physics: Conference Series, 1618, 062 015, https://doi.org/10.1088/1742-6596/1618/6/062015, 2020.

Taruffi, F., Combette, R., and Viré, A.: Experimental and CFD analysis of a floating offshore wind turbine under imposed motions, in: Journal of Physics: Conference Series, vol. 2767, p. 062010, IOP Publishing, 2024a.

Taruffi, F., Novais, F., and Viré, A.: An experimental study on the aerodynamic loads of a floating offshore wind turbine under imposed motions, Wind Energy Science, 9, 343–358, https://doi.org/10.5194/wes-9-343-2024, 2024b.

Thys, M., Chabaud, V., Sauder, T., Eliassen, L., Sæther, L. O., and Magnussen, B.: Real-Time Hybrid Model Testing of a Semi-Submersible 10MW Floating Wind Turbine and Advances in the Test Method, in: ASME 2018 1st International Offshore Wind Technical Conference, American Society of Mechanical Engineers, ISBN 978-0-7918-5197-5, https://doi.org/10.1115/IOWTC2018-1081, 2018.

van Kuik, G. A. M., Peinke, J., Nijssen, R., Lekou, D., Mann, J., Sørensen, J. N., Ferreira, C., van Wingerden, J. W., Schlipf, D., Gebraad, P., Polinder, H., Abrahamsen, A., van Bussel, G. J. W., Sørensen, J. D., Tavner, P., Bottasso, C. L., Muskulus, M., Matha, D., Lindeboom, H. J., Degraer, S., Kramer, O., Lehnhoff, S., Sonnenschein, M., Sørensen, P. E., Künneke, R. W., Morthorst, P. E., and Skytte, K.: Long-term research challenges in wind energy – a research agenda by the European Academy of Wind Energy, Wind Energy Science, 1, 1–39, https://doi.org/10.5194/wes-1-1-2016, 2016.

Viselli, A. M., Goupee, A. J., and Dagher, H. J.: Model Test of a 1:8-Scale Floating Wind Turbine Offshore in the Gulf of Maine1, Journal of Offshore Mechanics and Arctic Engineering, 137, https://doi.org/10.1115/1.4030381, 2015.

Zhao, Y. s., She, X. h., He, Y. p., Yang, J. m., Peng, T., and Kou, Y. f.: Experimental Study on New Multi-Column Tension-Leg-Type Floating Wind Turbine, China Ocean Engineering, 32, 123–131, https://doi.org/10.1007/s13344-018-0014-0, 2018.